Baryon density correlations in high temperature hadronic matter

Claude Bernard
Department of Physics, Washington University, St. Louis, Missouri 63130

Thomas A. DeGrand
Physics Department, University of Colorado, Boulder, Colorado 80309

Carleton DeTar
Department of Physics, University of Utah, Salt Lake City, Utah 84112

Steven Gottlieb
Department of Physics, Indiana University, Bloomington, Indiana 47405

Alex Krasnitz
Interdisciplinary Project Center for Computing, ETH-Zentrum, CH-8092 Zurich, Switzerland

Robert L. Sugar
University of California, Santa Barbara, California 93106

Douglas Toussaint
Department of Physics, University of Arizona, Tucson, Arizona 85721
(Received 10 September 1993)

As part of an ongoing effort to characterize the high temperature phase of QCD, in a numerical simulation using the staggered fermion scheme, we measure the quark baryon density in the vicinity of a fixed test quark at high temperature and compare it with similar measurements at low temperature and at the crossover temperature. We find an extremely weak correlation at high temperature, suggesting that small color singlet clusters are unimportant in the thermal ensemble. We also find that at $T = 0.75\ T_c$ the total induced quark number shows a surprisingly large component attributable to baryonic screening. A companion simulation of a simple flux tube model produces similar results and also suggests a plausible phenomenological scenario: As the crossover temperature is approached from below, baryonic states proliferate. Above the crossover temperature the mean size of color singlet clusters grows explosively, resulting in an effective electrostatic deconfinement.

PACS number(s): 12.38.Gc, 12.38.Mh, 12.38.Aw, 24.85.+p

I. INTRODUCTION

Numerical simulations of the quark plasma have suggested seemingly contradictory models. While bulk thermodynamic quantities, such as the energy density [1] and baryon susceptibility [2] yield values consistent with a nearly free gas of quarks and gluons, measurements of screening propagators, particularly, measurements of the wave functions of exchanged objects, are consistent with the confinement of color singlets [3]. Indeed, simulations and analytic work in the pure glue sector have demonstrated that spacelike Wilson loops obey an area law in the high temperature phase, a signature of confinement [4].

One resolution of this seeming paradox describes the quark plasma as an ensemble of color singlet clusters of various sizes. Bulk thermodynamic quantities, such as the energy density, would receive contributions from all clusters, whereas long-range screening would be controlled by the lightest clusters. How large is the typical color singlet cluster? What is the typical spatial extent and quark and antiquark content? To answer these questions, it is necessary to seek observables that have not hitherto been studied in this context. Thus, we measured the distribution of induced quark charge (baryon number) in the vicinity of a fixed test quark, at low and high temperature, and at the crossover temperature. This observable has also been studied by Müller and co-workers in an effort to discern changes in the QCD vacuum induced by color charges [5]. At low temperature we expect that, as a result of confinement, a dynamical antiquark or, less often, a pair of quarks, screens the test charge at short distance. Thus, the induced dynamical quark number density should be large and negative close to the test charge. If screening is entirely due to a single antiquark, we should observe that the total induced quark number Q is -1. By contrast, if color singlet clusters are large either in size or in the number of quarks and antiquarks, we would expect only a small induced charge density near the source.

In Sec. II we describe the observable in detail, and in

Sec. III we present the results of the numerical simulation. Among the more striking results is the surprising weakness of the induced quark number density at high temperature. We also find that at temperatures near, but below, the crossover, the total induced charge is significantly different from what would be expected if only a single antiquark were responsible for screening [6].

To help understand these results we turned to a simple flux tube model of Patel [7]. This model incorporates some of the essential features of QCD but has the added appeal that it can be formulated simply, either in a field-diagonal basis analogous to the Wilson QCD action or in a phenomenologically suggestive flux-diagonal basis. The latter representation permits the study of the growth and complexity of the color singlet clusters of the model. The induced quark density and charge can also be studied in this model. Results of this study are presented in Sec. IV. We find results surprisingly similar to those for QCD. A direct examination of color singlet cluster size in this model suggests an explanation for the QCD results, including a description of the nature of the phase transition, and of the structure of the high temperature phase. In particular, it suggests that heating of the confined phase results in the appearance of quark clusters, including a surprisingly high number of baryons and antibaryons. As the crossover temperature is passed, these clusters grow explosively, both in size and in quark content, resulting in a suppression of baryonic correlations, a rise in the baryon susceptibility, and an effective electrostatic deconfinement. A concluding discussion is given in Sec. V.

II. INDUCED BARYON DENSITY FOR STAGGERED FERMIONS

Here we derive the staggered fermion observables to be measured in the numerical simulation.

A. Baryon density from the local chemical potential

The construction of the local quark number density starts with the introduction of a baryon chemical potential in the standard way [8], but with a spatial dependence. Such a definition assures that the total baryon charge so defined is exactly conserved on the lattice. We start with the lattice action for staggered fermions in the notation of Ref. [2], modified through the introduction of a *local* chemical potential. Let $r = (\mathbf{r}, t)$ and $r' = (\mathbf{r}', t')$ denote lattice coordinates. The action is

$$S(U, \psi, \bar{\psi}) = S_g(U) + \sum_{r,r'} \bar{\psi}(r) M(U)_{r,r'} \psi(r') \ , \qquad (1)$$

where $S_g(U)$ is the pure gauge action. The fermion flavor is implicitly summed over. The fermion matrix for a single flavor with a local chemical potential $\mu(\mathbf{r})$ is given by

$$\begin{aligned} M(U)_{r,r'} = {} & 2ma\delta_{r,r'} \\ & + \sum_{\nu \in \{\hat{x},\hat{y},\hat{z}\}} [\tilde{U}_{r,\nu}\delta_{r,r'-\nu} - \tilde{U}^{\dagger}_{r-\nu,\nu}\delta_{r,r'+\nu}] \\ & + M^t(U)_{r,r'} \ , \end{aligned} \qquad (2)$$

where the link matrices include the usual Dirac phase factor

$$\tilde{U}_{r,\nu} = \eta_{r,\nu} U_{r,\nu} \ . \qquad (3)$$

The Dirac phase factors $\eta_{r,t}$ also include the sign for the antiperiodic boundary condition. We consider two alternative formulations "static" and "slice" for the time-hopping part of the fermion matrix M^t. First

$$M^t_{\text{static}}(U)_{r,r'} = [\tilde{U}_{r,t} e^{a\mu(\mathbf{r})} \delta_{r,r'-\hat{t}} - \tilde{U}^{\dagger}_{r-t,\hat{t}} e^{-a\mu(\mathbf{r})} \delta_{r,r'+\hat{t}}] \ . \qquad (4)$$

Notice that the fugacity factor has been spread uniformly in the time dimension. We also consider an alternative "single-slice" definition that introduces the fugacity factor on a single time slice:

$$M^t_{\text{slice}}(U)_{r,r'} = [\tilde{U}_{r,t} e^{N_t a\mu(\mathbf{r})} \delta_{r,r'-\hat{t}} \delta_{t',0} - \tilde{U}^{\dagger}_{r-t,\hat{t}} e^{-N_t a\mu(\mathbf{r})} \delta_{r,r'+\hat{t}} \delta_{t,0}] + [\tilde{U}_{r,t} \delta_{r,r'-\hat{t}} (1 - \delta_{t',0}) - \tilde{U}^{\dagger}_{r-\hat{t},t} \delta_{r,r'+\hat{t}} (1 - \delta_{t,0})]. \qquad (5)$$

Of course, which formulation we choose depends on what we want to measure. If the chemical potential $\mu(\mathbf{r})$ is introduced on a single time slice as in Eq. (5), it is a source for the local baryon density at a single time. If it is instead spread over all time as in Eq. (4), it is a source for the time-averaged (static) baryon density. When $\mu(\mathbf{r})$ is independent of $\mathbf{r}$ it can be shown that the determinant of the fermion matrix is the same in either case. Thus, for example, the baryon susceptibility [2] is obtained by differentiating the free energy twice with respect to such a constant chemical potential, so it is the same in either formulation. Moreover, for any local time-independent observable, such as the baryon density in the presence of a static charge, the expectation value is the same. A difference appears in the dynamical baryon density-density correlation, which may depend on the time separation

of the operators. The single-slice formulation gives the equal-time density-density correlation, and the static formulation gives the correlation of the time-averaged densities. For those observables that are independent of the formulation, we find that the static version has the practical advantage that, because of time averaging, it produces a higher signal to noise ratio.

The baryon density per unit lattice cell a^3 at zero chemical potential at a chosen spatial coordinate $\mathbf{r}$ is given in terms of the individual flavor densities by

$$\rho(\mathbf{r}) = \sum_{i=1}^{N_f} \rho_i(\mathbf{r}) \tag{6}$$

where

$$\rho_i(\mathbf{r}) = \beta^{-1}\partial \ln Z/\partial\mu_i(\mathbf{r})|_{\mu_i(\mathbf{r})=0}. \tag{7}$$

Here $\beta = 1/T$. Now, for two flavors of staggered fermions the partition function is

$$Z = \int [dU] \exp[-S_g(U)][\det M_u(U,\mu_u) \times \det M_d(U,\mu_d)]^{1/4} , \tag{8}$$

and we have

$$\langle\rho_{u,d}(\mathbf{r})\rangle = (4\beta)^{-1} \left\langle \mathrm{Tr}[M_{u,d}^{-1}\partial M_{u,d}/\partial\mu_{u,d}(\mathbf{r})]\right\rangle_U |_{\mu_{u,d}(\mathbf{r})=0} . \tag{9}$$

The result is

$$\langle\rho_{u,d}(\mathbf{r})\rangle = (1/4)\phi_\tau \Big\langle \mathrm{Tr}_c[M^{-1}_{(\mathbf{r},\tau+1),(\mathbf{r},\tau)}\tilde{U}_{(\mathbf{r},\tau);t}] + \mathrm{Tr}_c[M^{-1}_{(\mathbf{r},\tau),(\mathbf{r},\tau+1)}\tilde{U}^\dagger_{(\mathbf{r},\tau);t}]\Big\rangle_U , \tag{10}$$

where τ is summed over and Tr_c denotes a trace over color indices only. As a device for treating both static and slice cases for the time-hopping term in the same expression, we have introduced the weight

$$\phi_{\mathrm{static},\tau} = 1/N_t , \quad \phi_{\mathrm{slice},\tau} = \delta_{\tau,0}. \tag{11}$$

Because the hopping term in the staggered fermion matrix has the time-reversal symmetry

$$M^{-1}_{r,r'} = (-)^{r-r'} M^{-1\dagger}_{r',r} , \tag{12}$$

the two terms on the right-hand side (RHS) of the expression for the density are negative complex conjugates of each other. We get

$$\langle\rho_{u,d}(\mathbf{r})\rangle = (i/2)\mathrm{Im}\,\langle P_{\mathrm{dyn}}(\mathbf{r})\rangle , \tag{13}$$

where

$$P_{\mathrm{dyn}}(\mathbf{r}) = \mathrm{Tr}_c\left[M^{-1}_{(\mathbf{r},\tau+1),(\mathbf{r},\tau)}\tilde{U}_{(\mathbf{r},\tau);t}\phi_\tau\right]. \tag{14}$$

Clearly for the particular time-independent case of Eq. (13) both the single-slice and static formulations yield the same result. In particular, since the expectation value on the RHS is related to the Polyakov loop expectation value, which is real for the usual action at zero chemical potential, we get zero for the baryon density at zero chemical potential, as we should.

B. Density in the presence of a test quark

Now we want to consider the correlation between a point test quark at the origin (say) and the baryon density at $\mathbf{r}$. Introducing the test quark simply involves modifying the action by including a Polyakov loop factor $P_{\mathrm{fixed}}(0)$, defined through

$$P_{\mathrm{fixed}}(\mathbf{r}) = \mathrm{Tr}_c\left[\prod_{t=0}^{N_t}\tilde{U}_{(\mathbf{r},t);t}\right]. \tag{15}$$

We then have the partition function for the ensemble with the test quark:

$$Z_q = \int [dU]\exp[-S_g(U)] \times [\det M_u(U,\mu_u)\det M_d(U,\mu_d)]^{1/4} P_{\mathrm{fixed}}(\mathbf{0}) . \tag{16}$$

The baryon density $\rho_q(\mathbf{r})$ in the presence of the fixed quark can be calculated on the original ensemble Z through

$$\rho_q(\mathbf{r}) = (iN_f/2)\,\langle P_{\mathrm{fixed}}(0)\mathrm{Im}P_{\mathrm{dyn}}(\mathbf{r})\rangle_U / \langle P_{\mathrm{fixed}}(0)\rangle_U . \tag{17}$$

Now the expectation values are taken with respect to the original test-charge-free ensemble. The correlation between $\mathrm{Re}P_{\mathrm{fixed}}$ and $\mathrm{Im}P_{\mathrm{dyn}}$ vanishes because of the complex conjugation symmetry of the integral over the gauge variables. What survives is the correlation of the imaginary parts divided by the expectation of the real part of the Polyakov loop: namely,

$$\rho_q(\mathbf{r}) = -(N_f/2)\frac{\langle\mathrm{Im}P_{\mathrm{fixed}}(\mathbf{0})\mathrm{Im}P_{\mathrm{dyn}}(\mathbf{r})\rangle_U}{\langle\mathrm{Re}P_{\mathrm{fixed}}(\mathbf{0})\rangle_U} . \tag{18}$$

C. Density-density correlation

The connected density-density correlation for flavors i and j is given by

$$\rho_{ij}(\mathbf{r}) = \langle\rho_i(\mathbf{r})\rho_j(\mathbf{0})\rangle - \langle\rho_i(\mathbf{0})\rangle\langle\rho_j(\mathbf{0})\rangle = \beta^{-2}\partial^2 \log Z/\partial\mu_i(\mathbf{r},0)\partial\mu_j(\mathbf{0},0)|_{\mu_i(\mathbf{r})=0} . \tag{19}$$

In terms of the integrated correlation

$$\rho_{\mathrm{tot},ij} = \int d^3r\,\rho_{ij}(\mathbf{r}) \tag{20}$$

the baryon singlet and nonsinglet susceptibilities [2] are

$$\chi_S = \beta(\rho_{\mathrm{tot},uu} + \rho_{\mathrm{tot},dd} + \rho_{\mathrm{tot},ud} + \rho_{\mathrm{tot},du}) \ , \tag{21}$$

$$\chi_{NS} = \beta(\rho_{\mathrm{tot},uu} + \rho_{\mathrm{tot},dd} - \rho_{\mathrm{tot},ud} - \rho_{\mathrm{tot},du}) \ . \tag{22}$$

In terms of the fermion matrices for the separate flavors the correlation receives four contributions

$$\rho_{ij}(\mathbf{r}) = S_{11ij} + S_{21ij} + S_{22ij} - S_{\mathrm{disc},ij} \ . \tag{23}$$

The indices nm in S_{nmij} count the number of explicit coordinate points n and number of color traces m:

$$S_{11ij} = (2\beta)^{-2}\delta_{ij} \left\langle \mathrm{Tr}[M_i^{-1}\partial^2 M_i/\partial\mu_i(\mathbf{r})\partial\mu_i(\mathbf{0})] \right\rangle_U |_{\mu_{u,d}(\mathbf{r})=0} \ , \tag{24}$$

$$S_{21ij} = -(2\beta)^{-2}\delta_{ij} \left\langle \mathrm{Tr}[M_i^{-1}\partial M_i/\partial\mu_i(\mathbf{r}) M_i^{-1}\partial M_i/\partial\mu_i(\mathbf{0})] \right\rangle_U |_{\mu_{u,d}(\mathbf{r})=0} \ , \tag{25}$$

$$S_{22ij} = (4\beta)^{-2} \left\langle \mathrm{Tr}[M_i^{-1}\partial M_i/\partial\mu_i(\mathbf{r})]\mathrm{Tr}[M_j^{-1}\partial M_j/\partial\mu_j(\mathbf{0})] \right\rangle_U |_{\mu_{u,d}(\mathbf{r})=0} \ , \tag{26}$$

$$S_{\mathrm{disc}ij} = \langle\rho_i(\mathbf{0})\rangle \langle\rho_j(\mathbf{0})\rangle \ . \tag{27}$$

Carrying out the derivatives and using the time-reversal property (12) gives

$$S_{11ij} = 2^{-1}\delta_{ij}\delta_{\mathbf{r},\mathbf{0}} \langle \mathrm{Re}P_{\mathrm{dyn}}(\mathbf{0})\rangle \ , \tag{28}$$

$$\begin{aligned} S_{21ij} = {} & -2^{-1}\delta_{ij}\phi_{\tau'}\phi_\tau \left\langle \mathrm{ReTr}_c[M^{-1}_{(\mathbf{0},\tau+1),(\mathbf{r},\tau')}\tilde{U}_{(\mathbf{r},\tau');t} M^{-1}_{(\mathbf{r},\tau'+1),(\mathbf{0},\tau)}\tilde{U}_{(\mathbf{0},\tau);t}] \right\rangle_U \\ & -2^{-1}\delta_{ij}\phi_{\tau'}\phi_\tau \left\langle \mathrm{ReTr}_c[M^{-1}_{(\mathbf{0},\tau+1),(\mathbf{r},\tau'+1)}\tilde{U}^\dagger_{(\mathbf{r},\tau');t} M^{-1}_{(\mathbf{r},\tau'),(\mathbf{0},\tau)}\tilde{U}_{(\mathbf{0},\tau);t}] \right\rangle_U \ , \end{aligned} \tag{29}$$

$$S_{22ij} = -4^{-1} \langle \mathrm{Im}P_{\mathrm{dyn}}(\mathbf{r})\mathrm{Im}P_{\mathrm{dyn}}(\mathbf{0})\rangle_U \ . \tag{30}$$

The two-point single-trace term S_{21ij} is a hadron propagator with a source at $(\mathbf{0},\tau)$ and a sink at $(\mathbf{r},\tau')$. The source and sink are both just the point-split baryon density operator. To evaluate this term we require the quark propagator from the source $\tilde{U}_{(\mathbf{0},\tau);t}$ at $(\mathbf{0},\tau)$ and the antiquark propagator from a point source at $(\mathbf{0},\tau+1)$. These propagators are combined in two ways at $(\mathbf{r},\tau')$ to complete the evaluation of the two contributions.

To evaluate the two-point, two-trace term S_{22ij} we use the random source trick of Ref. [2]. We introduce a set of n_{rand} independent complex Gaussian random SU(3) vectors $R_\ell(\mathbf{r},\tau)$ $\ell = 1,\ldots,n_{\mathrm{rand}}$ on the time slice $\tau = 1$ for the slice form of the action and for all τ for the static form. Then on a given gauge configuration U we generate the Fourier transform of the estimate of $\mathrm{Im}P_{\mathrm{dyn}}(\mathbf{r})$:

$$I_{\mathrm{dyn},\ell}(\mathbf{k}) = \sum_{\mathbf{r}} \exp(i\mathbf{r}\cdot\mathbf{k})\phi_\tau \mathrm{Im}[R_\ell(\mathbf{r})^* M^{-1}_{(\mathbf{r},\tau+1),(\mathbf{r},\tau)}\tilde{U}_{(\mathbf{r},\tau),t}R_\ell(\mathbf{r})]. \tag{31}$$

(Note that the imaginary part is taken before carrying out the Fourier transform.)

Finally, we estimate the Fourier transform of S_{22ij} from

$$S_{22ij}(\mathbf{k}) = -\frac{1}{4n_{\mathrm{rand}}(n_{\mathrm{rand}}-1)} \sum_{\ell\neq\ell'} \left\langle I^*_{\mathrm{dyn},\ell}(\mathbf{k}) I_{\mathrm{dyn},\ell'}(\mathbf{k}) \right\rangle_U . \tag{32}$$

The single-point, single-trace term can be generated trivially from the random source method through the estimate

$$S_{11ij} = \frac{\delta_{ij}\delta_{\mathbf{r},\mathbf{0}}}{2n_{\mathrm{rand}}V} \sum_\ell \sum_{\mathbf{r}} \mathrm{Re}[R_\ell(\mathbf{r},\tau)^* M^{-1}_{(\mathbf{r},\tau+1),(\mathbf{r},\tau)}\tilde{U}_{(\mathbf{r},\tau),t}R_\ell(\mathbf{r},\tau)]. \tag{33}$$

Thus the computation of S_{11ij} and S_{22ij} starts with the evaluation of the quark propagator from the same parallel-transported random source, namely, $\tilde{U}_{(\mathbf{r},\tau),t}R_k(\mathbf{r},\tau)$. The same Fourier transform $I_{\mathrm{dyn},i}$ is used to obtain the correlation with the static source. However, evidently the computation of the hadron propagator S_{21ij} must be done with point sources—not random sources.

III. RESULTS OF SIMULATIONS

Simulations were carried out at fixed $6/g^2 = 5.445$ and quark mass $am_q = 0.025$ for two flavors of staggered fermions on lattices of size $16^3 \times N_t$, where $N_t = 8, 6, 4$. This choice of lattice parameters corresponds to the crossover temperature at $N_t = 6$ [9]. Thus, the simula-

tions are done at three temperatures $T = 0.75T_c$, $T \approx T_c$, and $T = 1.5T_c$, respectively, at the *same* lattice scale, making it meaningful to superimpose plots of baryon density vs distance from the source. Spectroscopic simulations at the same temperature [10] allow us to set the scale, viz., $T_c = 145$ MeV and $a = 0.227$ fm. Simulations were also carried out at $N_t = 4$ with $6/g^2 = 5.15$, 5.22, 5.25, and 5.29 (the crossover) to provide an independent check of trends in the total induced quark number. Table I shows the extent of the simulation sample.

Figure 1 summarizes our results for the induced quark number density at these three temperatures. Particularly striking is the dramatic decrease in the correlation at high temperature. Thus, we see no evidence for small color singlet clusters in the high temperature plasma.

The total induced quark number normalized to one for a single quark was computed in two ways: first by a direct integration of the density (18) and second by fitting the density distribution to the functional form

$$\rho_q(\mathbf{r}) = \sum_j \sum_{\mathbf{k}} e^{2\pi i \mathbf{k}\cdot\mathbf{r}/N} \frac{a_j}{\sum_{i=1}^{3} 2\cos(2\pi k_i/N) + m_j^2 - 6}, \tag{34}$$

(the sum of free lattice propagators for scalar fields of mass m_j) from which the total induced quark number is

$$Q = N^3 \sum_j a_j/m_j^2. \tag{35}$$

At most two mass terms were used. All fits started at zero radius. The resulting total quark number determined from the two methods was in each case consistent within errors. The value quoted is the one with the smaller standard deviation. It was found that except for the high temperature points ($6/g^2 = 5.445$, $N_t = 4$ and $6/g^2 = 5.29$, $N_t = 6$) direct summation over the entire volume gave poorer statistics than fitting because direct summation suffers from statistical noise introduced by contributions far from the fixed charge that should sum to zero. By fitting to a functional form that falls to zero at infinity, we controlled this noise.

The resulting fitted curves are plotted in Fig. 1. The total quark number values are also given in the legend and in Table II. At the high temperature point the total induced quark number is nearly two orders of magnitude smaller than the quark number at low temperature. At low temperature we expect that the test charge is attached to a color singlet cluster. A single antiquark would contribute -1 to the total induced quark number, and a pair of quarks forming a baryon, $+2$. A thermodynamic mixture of these two configurations would give an intermediate value. Based on the error ellipse for a two-parameter fit to the lowest temperature density, at the two standard deviation level, we find that the total induced quark number is greater than -0.55, significantly different from -1.

TABLE I. QCD simulation sample size (molecular dynamics time units).

$6/g^2$	N_t	Time
5.15	4	994.5
5.22	4	856
5.25	4	430
5.29	4	500
5.445	4	611
5.445	6	1141
5.445	8	2665

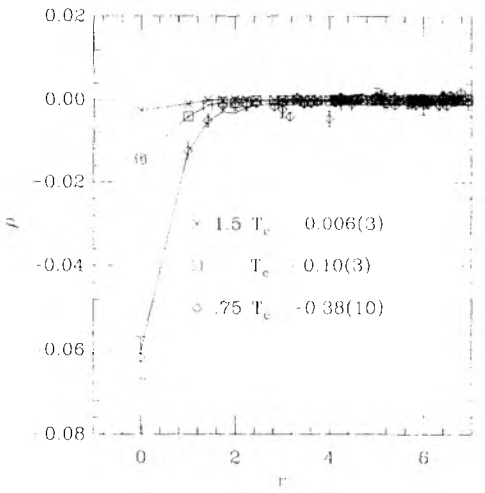

FIG. 1. Quark number density induced by a fixed quark at the origin as a function of distance from the origin at three temperatures. Curves are fits to a single screening mass. The total induced quark number Q is also shown.

As a check of this result, we also carried out a series of simulations at varying $6/g^2$ with $N_t = 4$. At such a strong coupling the Polyakov loop expectation value is large, leading to a stronger signal in the correlation. Results for the induced quark number are plotted in Fig. 2 and listed in Table III. The low temperature values are somewhat larger in magnitude than in the $6/g^2 = 5.445$ simulation but still show a significant departure from -1.

For the sake of comparison let us estimate the contribution to the induced charge from the lowest S-wave

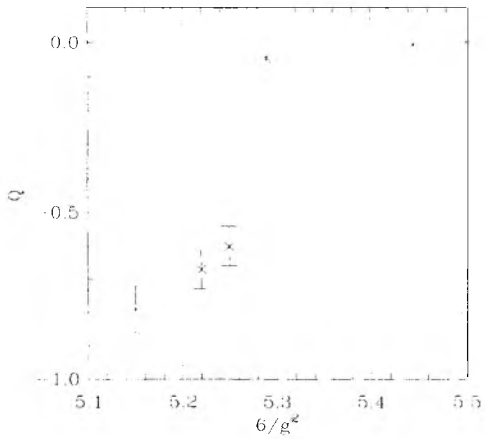

FIG. 2. Total induced quark number vs $6/g^2$ at $N_t = 4$.

TABLE II. QCD simulation results for $6/g^2 = 5.445$.

					Static		Slice	
N_t	T/T_c	Q	ReP	$\langle\bar{\psi}\psi\rangle$	χ_s	χ_{ns}	χ_s	χ_{ns}
4	1.5	−0.380(100)	0.6480(20)	0.0768(5)	0.233(10)	0.2410(80)	0.240(20)	0.239(13)
6	1.0	−0.130(60)	0.1070(40)	0.3150(30)	0.030(7)	0.0360(40)	0.035(16)	0.042(13)
8	0.75	−0.006(3)	0.0065(5)	0.1860(5)	0.009(5)	0.0019(6)	0.010(12)	0.008(10)

mesonic and baryonic screening clusters in the ensemble. These clusters are obtained by replacing one quark in the π, ρ, N, and Δ by a fixed spinless, flavorless color triplet quark. The result is a modified $J = 1/2$, $I = 1/2$ meson with a fourfold multiplicity $g_{\rho'} = 4$, a modified $J = 0$, $I = 0$ "nucleon" N' and a modified $J = 1$, $I = 1$ delta Δ'. In the continuum limit the degeneracies are $g_{N'} = 1$ and $g_{\Delta'} = 9$. However, at finite lattice spacing the Δ' is split, owing to the discrete nature of the internal symmetries in the staggered fermion scheme. We have not measured masses of the modified states but have masses for their light quark counterparts [10] for the same coupling $6/g^2 = 5.445$, namely, $am_\rho = 0.918$, $am_\pi = 0.4488$, $am_N = 1.375$, and $am_\Delta = 1.43$. If we assume that the splitting of the ρ and π is entirely due to the color hyperfine interaction, then we estimate the mass of the modified meson to be $m_{\rho'} = M + (3m_\rho + m_\pi)/4 = M + 0.80/a$, where M represents the contribution from the point charge. Similarly, we have $m_{N'} = M + m_N = M + 1.375/a$ and $m_{\Delta'} = M + (2m_\Delta + m_N)/3 = M + 1.41/a$. To be conservative, let us assume that the Δ' is fully degenerate. As noted before, the induced quark number is

$$Q = -p_m + 2p_b, \tag{36}$$

where p_m and p_b are the probabilities of screening via the mesonic and baryonic clusters. For this estimate we take $p_m + p_b = 1$. The probabilities are estimated from the Boltzmann weights:

$$p_m/p_b = \frac{g_{\Delta'}e^{-m_{\Delta'}/T} + g_{N'}e^{-m_{N'}/T}}{g_{\rho'}e^{-m_{\rho'}/T}} = \frac{9e^{-1.41/aT} + e^{-1.375/aT}}{4e^{-0.80/aT}}. \tag{37}$$

The unknown regularization-dependent energy M has cancelled in the ratio. The resulting estimates are $Q = -0.94$ at $T = 0.75\ T_c = 1/8a$ and $Q = -0.81$ at $T = T_c = 1/6a$. These values are considerably lower than were found in the simulation. To bring the estimates into closer agreement would require adding more baryonic states. Thus the full simulation suggests that already at a temperature of $0.75\ T_c$, there is significant baryonic screening of the fixed charge.

As we have remarked (22), the integral of the self-correlation of the dynamical quark number density gives the baryon susceptibility. Results for the susceptibility on $8^3 \times 4$ lattices with $ma = 0.025$ were reported in Ref. [2]. The high temperature values found are consistent with what would be expected for an ideal quark gas, given the very large effects of the nonzero lattice spacing. As a check, we compare our new results on $16^3 \times 4$. Figures 3 and 4 show the comparison for the $N_t = 4$ series. They are apparently consistent. Results for the $N_t = 4$ series are also given in Table III and for the $6/g^2 = 5.445$

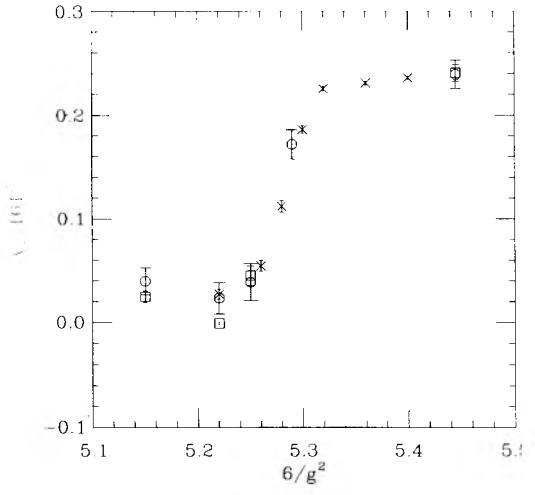

FIG. 3. Nonsinglet quark number susceptibility vs $6/g^2$ at $N_t = 4$ with bare quark mass $ma = 0.025$, compared with Ref. [2] (crosses). Two forms of the quark number density are used: "static" (squares) and "slice" (circles).

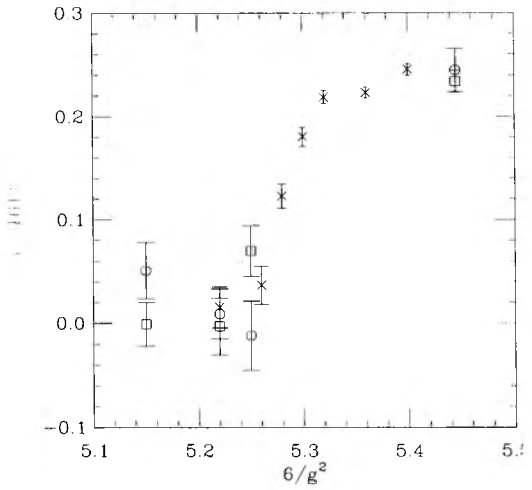

FIG. 4. Singlet quark number susceptibility vs $6/g^2$ at $N_t = 4$ with bare quark mass $ma = 0.025$. Symbols are as in the previous figure.

TABLE III. QCD simulation results for $N_t = 4$.

				Static		Slice	
$6/g^2$	Q	ReP	$\langle\bar{\psi}\psi\rangle$	χ_s	χ_{ns}	χ_s	χ_{ns}
5.15	−0.790(70)	0.0486(9)	0.4945(10)	0.000(20)	0.025(6)	0.05(3)	0.040(13)
5.22	−0.670(60)	0.0680(20)	0.4477(13)	0.000(30)	0.000(1)	0.01(2)	0.023(15)
5.25	−0.600(60)	0.0860(20)	0.4110(20)	0.070(20)	0.045(9)	−0.01(3)	0.039(18)
5.29	−0.046(6)	0.4060(20)	0.1990(30)				0.171(14)
5.445	−0.006(3)	0.6480(20)	0.0768(5)	0.233(10)	0.241(8)	0.24(2)	0.239(13)

series, in Table II. Not surprisingly, the static form of the density operator gives a better signal than the single time slice form because it involves an average over all time links. Values are not available for $6/g^2 = 5.29$, which was run before improvements in the code incorporated the static form and gave an acceptable signal to noise ratio for the slice form.

The correlation between a test charge and the scalar density $\langle\bar{\psi}\psi\rangle$ has been measured by Müller and coworkers [5]. Our results, shown in Fig. 5, are consistent with theirs.

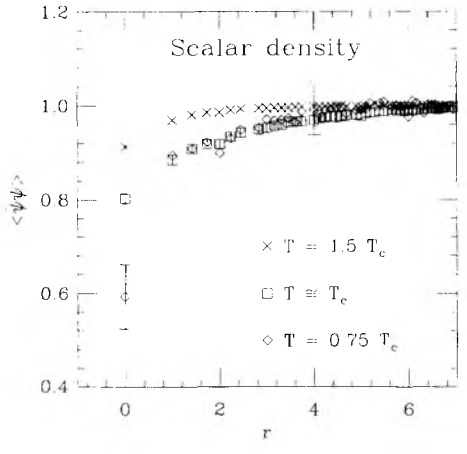

FIG. 5. Scalar density correlation $\langle\bar{\psi}\psi\rangle$ vs distance from a point charge, normalized to one at infinite distance. Error bars for the two lowest temperature points are as small or smaller than the plot symbol. For the sake of clarity, for the highest temperature only two typical error bars are shown.

IV. FLUX TUBE MODEL

A. The model

Some years ago Patel [7] proposed a flux tube version of the three-state three-dimensional Potts model to explain the mechanism of the deconfining phase transition in QCD. In this model, each site $\mathbf{r}$ of a cubic lattice holds either a quark, antiquark, or none at all, and each link $\ell_{\mathbf{r},\mu}$, a triplet or antitriplet flux, or none at all. That is the quark number $n_{\mathbf{r}}$ and the flux $\ell_{\mathbf{r},\mu}$ take on values $\{-1, 0, 1\}$. Flux is conserved modulo 3:

$$\sum_{\mu=1}^{3} \ell_{\mathbf{r},\mu} + \ell_{\mathbf{r},-\mu} - n_{\mathbf{r}} = 0 \bmod 3 \tag{38}$$

where $\ell_{\mathbf{r},-\mu} = -\ell_{\mathbf{r}-\hat{\mu},\mu}$. The Hamiltonian is given in terms of the quark mass m and the string link energy σ by

$$H = \sum_{\mathbf{r},\mu} \sigma|\ell_{\mathbf{r},\mu}| + \sum_{\mathbf{r}} m|n_{\mathbf{r}}|. \tag{39}$$

The partition function is then

$$Z(\beta) = \sum_{\{\ell_{\mathbf{r},\mu}, n_{\mathbf{r}}\}'} \exp(-\beta H) \ , \tag{40}$$

where the prime signifies a sum constrained by (38).

B. Equivalence to the Potts model

This model is equivalent to the three-state three-dimensional Potts model [7]. The equivalence can be seen by replacing the Gauss' law constraint by

$$\delta_{\ell,0} = \frac{1}{3} \sum_{z \in Z(3)} z^{\ell} \tag{41}$$

in modulo three arithmetic. Here $Z(3) = \{1, e^{\pm 2\pi i/3}\}$. Introducing this identity on each site with the summation variable $z_{\mathbf{r}}$ allows us to rewrite the partition function as

$$Z(\beta) = \sum_{\{\ell_{\mathbf{r},\mu}, n_{\mathbf{r}}, z_{\mathbf{r}}\}} \exp\left(-\beta\left[\sum_{\mathbf{r},\mu} \sigma|\ell_{\mathbf{r},\mu}| + \sum_{\mathbf{r}} m|n_{\mathbf{r}}|\right]\right) \times \prod_{\mathbf{r}} z_{\mathbf{r}}^{\sum_{\mu}(\ell_{\mathbf{r},\mu}+\ell_{\mathbf{r},-\mu})-n_{\mathbf{r}}} \ . \tag{42}$$

The unconstrained sums over links and quark numbers can be carried out as follows:

$$\sum_{\ell_{\mathbf{r},\mu}} \exp(-\beta|\ell_{\mathbf{r},\mu}|)(z_{\mathbf{r}} z^*_{\mathbf{r}+\hat{\mu}})^{\ell_{\mathbf{r},\mu}} = 1 + 2\mathrm{Re}(z_{\mathbf{r}} z^*_{\mathbf{r}+\hat{\mu}}) \times \exp(-\beta\sigma) \ , \tag{43}$$

$$\sum_{n_{\mathbf{r}}} \exp(-\beta m|n_{\mathbf{r}}|) z_{\mathbf{r}}^{-n_{\mathbf{r}}} = 1 + 2\mathrm{Re} z_{\mathbf{r}} e^{-\beta m}. \tag{44}$$

Thus the partition function reduces to a product of polynomials in the $Z(3)$ variables $z_{\mathbf{r}}$. A Hamiltonian can be constructed through the identity over $Z(3)$:

$$\ln(1 + cz + cz^*) = a + bz + bz^* \ , \tag{45}$$

where

$$\exp(3a) = (1 + 2c)(1 - c)^2 \ ,$$
$$\exp(3b) = (1 + 2c)/(1 - c) \ . \tag{46}$$

Thus if we define

$$J\beta' = \frac{2}{3} \ln \left(\frac{1 + 2\exp(-\beta\sigma)}{1 - \exp(-\beta\sigma)} \right) \ , \tag{47}$$

$$h\beta' = \frac{2}{3} \ln \left(\frac{1 + 2\exp(-\beta m)}{1 - \exp(-\beta m)} \right) , \tag{48}$$

then we have, up to a constant

$$Z(\beta) = \sum_{\{z_{\mathbf{r}}\}} \exp(-\beta' H') \ , \tag{49}$$

where

$$H' = -\sum_{\mathbf{r}\mu} J\mathrm{Re}(z_{\mathbf{r}} z^*_{\mathbf{r}+\hat{\mu}}) - \sum_{\mathbf{r}} h\mathrm{Re}z_{\mathbf{r}} . \tag{50}$$

This expression is recognized as the Hamiltonian of the three-state Potts model in three dimensions with a coupling J and a magnetic field h coupled to the real part of the spin.

Thus a low quark mass corresponds to a high Potts magnetic field and a low flux-model temperature corresponds to a high Potts temperature. At zero field h a first order phase transition is found in this model at $J\beta' \approx 0.367$. The phase transition persists for a small magnetic field $h\beta' < 0.002$ but is not evident in numerical simulations for larger values of the field [11]. These parameter values can be converted to the flux tube model values through the inverse of Eq. (48):

$$\beta\sigma = \ln \left(\frac{\exp(\frac{3}{2}J\beta') + 2}{\exp(\frac{3}{2}J\beta') - 1} \right) \ , \tag{51}$$

$$\beta m = \ln \left(\frac{\exp(\frac{3}{2}h\beta') + 2}{\exp(\frac{3}{2}h\beta') - 1} \right) , \tag{52}$$

giving a phase transition along a curve starting at about $\beta\sigma = 1.63$, $\beta m = \infty$ to about $\beta m > 6.9$ or $m/\sigma > 4.2$.

C. Relationship to QCD

Patel proposed using this model as a paradigm for the QCD phase transition. The Potts model in its more conventional form was also offered some years ago as a model of the deconfining phase transition [12]. The latter formulation is obtained from a high quark mass, strong coupling, high temperature, $Z(3)$-restricted approximation to the conventional field-diagonal Wilson action, with the Potts spin corresponding to the Polyakov loop. On the other hand the flux-tube formulation of the Potts model corresponds to an alternate representation of the Wilson action in the charge-and-flux-diagonal basis. Because of the combinatoric complexities of linking SU(3) charges and fluxes to form color singlets, such a basis for the Wilson action never received wide attention. However, in the simple $Z(3)$ basis of the flux tube model the combinatorics become trivial. Moreover, in the flux tube form the model offers the highly suggestive possibility of studying the size and structure of color singlet clusters as a function of temperature. Its chief drawback is that because it treats quarks as static objects it does not incorporate chiral symmetry.

At low temperature only small color singlet clusters populate the Gibbs ensemble. As the temperature is increased, clusters of increasing size occur. Eventually clusters connect to fill nearly the entire spatial volume. For heavy quark masses this phenomenon leads to a first-order deconfinement phase transition. For light quarks, cluster growth is somewhat inhibited, since pair formation breaks the flux links. It is found that there is no phase transition. One is tempted to think of a percolation phase transition mediated by the connectivity of the flux tubes, but there is nothing to percolate: there is no current in the model to flow between linked sites and establish long-range order. The first-order phase transition occurring only at large quark mass (low magnetic field) resembles more appropriately a liquid-gas phase transition.

D. Simulation and observables

To simulate the model in the flux tube basis, we used a Metropolis algorithm, with moves designed to preserve Gauss' law. We considered two types of elementary moves: the addition (or removal) of the lightest meson (flux link with quark and antiquark at the ends) and the addition (or removal) of the lightest "glueball" (four flux links directed around a plaquette). Adding was done in the literal sense: adding a quark to a site means increasing the quark number by one unit, modulo three, etc. Thus, the actual impact of these elementary moves depends on the configuration. The moves could result in shortening, lengthening, breaking, joining, or displacing a series of flux links. Notice that two or three such mesons can form a baryon, if they are added with the antiquark on the same site but with links and quarks on unique sites, so we did not create baryons through a separate move. Although by the same token four such mesons can form a glueball, since meson formation is suppressed at high quark mass, we kept both moves to allow a more efficient mass-independent coverage of the ensemble.

A fixed charge is introduced at the origin by starting from a modified vacuum configuration in which the dynamical quark charge at the origin is set to -1 and all other charges and fluxes are initially zero. Observables include the following: $|n|$ is the mean number of quarks plus antiquarks per site, $|\ell|$ the mean number of links (either sign) per link, n_{vtx} the mean number of three-point flux vertices, $\rho(\mathbf{r})$ the induced quark number density, Q the the total induced charge (quarks minus antiquarks), $\langle B^2 \rangle$ the mean square baryon number (including test charge), and N_0 the size of the cluster connected to the origin.

E. Results

Measurements were made on a 10^3 lattice for a variety of β at $m = 1.0$ (10 000 sweeps for each β value) and $m = 3.5$ (1000 sweeps for each β value). We use units in which $\sigma = 1$. As we have noted above, both quark masses are in a region where a phase transition does not occur. The higher mass series comes closer to the critical point. With such a small volume we would notice a significant finite-size rounding of the first-order phase transition that occurs at higher quark masses. However, we are primarily interested in the qualitative behavior of the model at smaller quark mass, since it corresponds more closely to the light quark QCD simulation. Thus the small volume suffices.

A popular indicator of the phase transition in QCD is the Polyakov loop ReP. The Potts model analogue is the magnetization:

$$\langle \mathrm{Re}z \rangle = \frac{\partial \ln Z}{\beta' \partial h} . \tag{53}$$

From the map Eq. (48) onto flux tube variables, we see that the flux tube analog of this order parameter is the mean quark count (quarks plus antiquarks)

$$\langle |n| \rangle = \frac{\partial \ln Z}{V \beta \partial m} . \tag{54}$$

Figures 6 and 7 show the quark number $|n|$ vs β for the two quark masses. The higher mass series comes closer to the critical point, leading to a sharper crossover. The crossover locations are determined from the inflection point of the curves (peak in the corresponding susceptibility) to be $1/T_c = \beta_c = 1.88(1)$ for $m = 1.0$ and $\beta_c = 1.662(2)$ for $m = 3.5$. These values are used to determine the ratio T/T_c in Tables IV and V.

Shown in Fig. 8 and Tables IV and V is the total induced charge Q as a function of β in the presence of a test charge for the two quark masses. The results bear a striking resemblance to those of the QCD simulation.

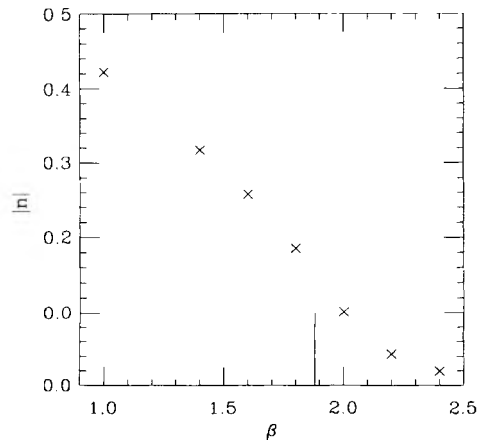

FIG. 6. Total number of quarks and antiquarks vs inverse temperature in the flux tube model for quark mass $m = 1.0$. The vertical line indicates the crossover.

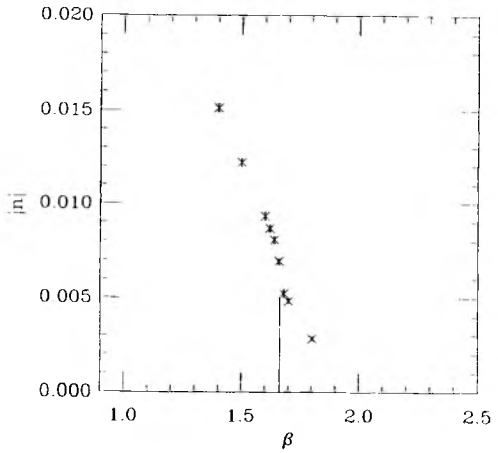

FIG. 7. Total number of quarks and antiquarks vs inverse temperature in the flux tube model for quark mass $m = 3.5$.

At high temperature, the induced charge is very small for both quark masses. For the heavier quark mass, the total induced charge $Q = -0.75(7)$ at the highest β ($T = 0.92\ T_c$) shows a significant departure from -1. For the lighter quark mass at the highest β ($T = 0.78\ T_c$) we also see a significant departure with $Q = -0.69(2)$.

Thus we find evidence of important baryonic screening in this model at temperatures close to the crossover. Is this surprising? Consider the relative Boltzmann weights for the lightest baryonlike and mesonlike clusters attached to the test quark. They are shown in Fig. 9. The masses are $m_m = M + m + \sigma$ and $m_b = M + 2m + 2\sigma$ for the mesonlike and baryonlike cluster, respectively. Here M stands for the mass of the fixed charge. For $m = 1$ and $\sigma = 1$, corresponding to the lighter quark mass, these are $m_m = M + 2$ and $m_b = M + 4$. The corresponding multiplicities are $g_m = 6$ and $g_b = 30$. At $\beta = 2.4$ we have, in the notation of Eq. (37),

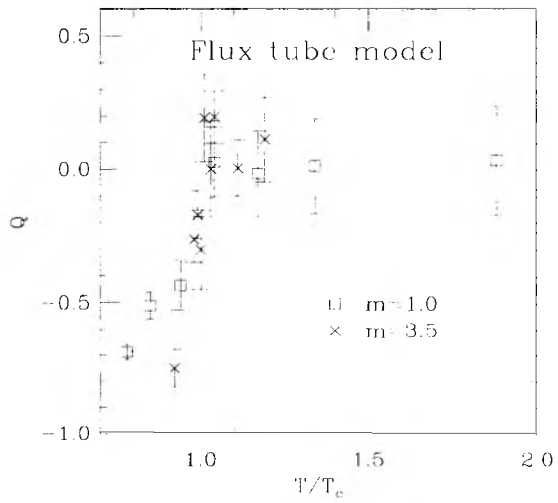

FIG. 8. Induced charge vs temperature in the flux tube model.

TABLE IV. Flux tube model results for $m = 1.0$.

β	T/T_c	$\lvert n\rvert$	$\lvert \ell \rvert$	$n_{\rm vtx}$	Q	$\langle B^2 \rangle$	N_0
1.0	1.88	0.42220(20)	0.42037(9)	157.550(80)	0.00(20)	46.50(60)	894(2)
1.4	1.34	0.31693(15)	0.30492(10)	105.580(70)	0.00(20)	35.00(50)	676(2)
1.6	1.17	0.25783(15)	0.23331(11)	73.680(80)	−0.01(15)	28.40(40)	430(3)
1.8	1.04	0.18532(15)	0.14651(12)	39.080(60)	0.03(13)	19.50(30)	73.5(1.0)
2.0	0.94	0.10102(14)	0.06091(10)	11.980(40)	−0.44(9)	9.53(13)	7.88(10)
2.2	0.85	0.04315(10)	0.01909(5)	2.490(20)	−0.51(5)	2.75(4)	3.25(3)
2.4	0.78	0.01957(7)	0.00714(3)	0.636(8)	−0.69(3)	0.834(15)	2.26(2)

$$p_b/p_m = 30e^{-4/T}/6e^{-2/T} = 0.04. \quad (55)$$

Thus, if only these two states played a role in low temperature screening we should find a total induced charge $Q = -0.88$, significantly different from what is observed. Clearly, still more baryonic states contribute. If we consider higher excitations, the number of distinct baryonic states (i.e., states with total baryon number $B \neq 0$) grows very rapidly with mass—much faster than mesonic states. Thus the entropy of baryon excitation increases the importance of baryonic screening. This point can be dramatized by a direct examination of configurations. Shown in Fig. 10 is a representative configuration obtained at the mass and inverse temperature in question: $m = 1$ and $\beta = 2.4$. It contains nine $q\bar{q}$ mesons, one qqq baryon, and one $\bar{q}\bar{q}\bar{q}$ antibaryon, a highly improbable occurrence in the naive two-state model.

Turning now to the induced density vs distance, we show results for the simulation at the lighter quark mass $m = 1.0$ in Fig. 11. Again we see a resemblance to results of the QCD simulation shown in Fig. 1. The total charge $Q(r \leq 3)$ given in the legend is found by integrating the density to an arbitrary cutoff distance $r \leq 3$. The correlation is stronger at low temperature than in the QCD simulation, reflecting a shorter correlation length in lattice units, which could be adjusted by a change of scale. From a fit to a single-pole lattice Yukawa form, we find an effective mass of 2.9(7) in the flux tube model at $\beta = 2.4$ and $m = 1.0$, to be compared with 1.7(6) for the corresponding low temperature curve for SU(3) (Fig. 1).

Further evidence of the importance of larger hadronic clusters can be obtained from a measurement of the mean size of the cluster attached to the origin. This size is defined as the number of sites connected through flux links to the origin. Our results are shown in Fig. 12. Notice that in this 10^3 lattice the mean cluster size grows dramatically, already filling 43% of the volume at $T \approx 1.2\,T_c$. Despite appearances, however, correlation lengths are nonetheless finite.

Another indicator of clustering is the number of three-point flux vertices $n_{\rm vtx}$. This statistic is the sum of one third the total flux entering each site, if the total flux count at the site is positive. With coordination number six a site can contribute only 0, 1, or 2 to this statistic. As can be seen from Tables IV and V this number grows with temperature in much the same way for both the smaller and larger quark mass. On the other hand, a striking difference is seen in the behavior of the baryon susceptibility $\langle B^2 \rangle / V$, as might be expected. For the lighter quark mass the fluctuation in baryon number is considerably larger at high temperature. The expected suppression of quark content with increasing quark mass is also evident in the quark number per site $|n|$. An expected consequence of decreasing quark mass is a decrease in cluster size, since pair creation breaks flux links. This effect is evident in the mean size of the cluster attached to the origin. At $m = 3.5$ and $\beta = 1.4$, corresponding to $T = 1.19\,T_c$, this mean size 650(3). When the quark mass is decreased to $m = 1.0$ at a comparable temperature ($\beta = 1.6$), the mean size decreases to 430(3). Thus, with decreasing quark mass the quark content of the clusters increases, and the size decreases somewhat.

V. CONCLUSIONS

In numerical simulations we have measured the quark number density in the vicinity of a test quark as a function of temperature. A strong correlation is found in the low temperature phase, but it is vastly reduced in the high temperature phase. We have also found evidence for a significant proliferation of baryonic clusters as the crossover temperature is approached from below.

TABLE V. Flux tube model results for $m = 3.5$.

β	T/T_c	$\lvert n\rvert$	$\lvert \ell \rvert$	$n_{\rm vtx}$	Q	$\langle B^2 \rangle$	N_0
1.40	1.19	0.0530(8)	0.2687(4)	71.1(3)	0.10(20)	1.77(6)	650(3)
1.50	1.11	0.0427(7)	0.2149(5)	51.3(2)	0.00(11)	1.35(7)	535(3)
1.60	1.04	0.0326(7)	0.1386(15)	27.9(4)	0.20(10)	1.09(7)	337(4)
1.62	1.03	0.0303(6)	0.1202(15)	22.7(4)	0.00(20)	0.97(6)	289(5)
1.64	1.01	0.0282(7)	0.0950(20)	16.5(5)	0.20(20)	0.94(6)	206(7)
1.66	1.00	0.0242(5)	0.0670(20)	10.1(4)	−0.30(15)	0.71(5)	117(5)
1.68	0.99	0.0183(7)	0.0450(20)	5.8(5)	−0.17(9)	0.54(5)	59(6)
1.70	0.98	0.0169(4)	0.0341(11)	3.8(2)	−0.26(9)	0.42(3)	35(3)
1.80	0.92	0.0099(3)	0.0137(3)	0.89(5)	−0.75(7)	0.12(3)	8.2(4)

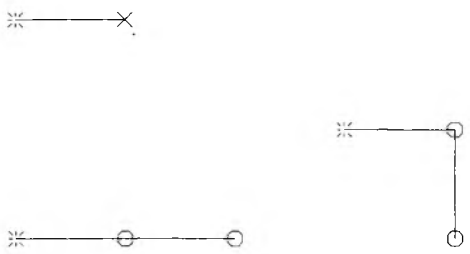

FIG. 9. Lightest mesonlike and baryonlike clusters (two types) attached to a fixed quark (burst) in the flux tube model.

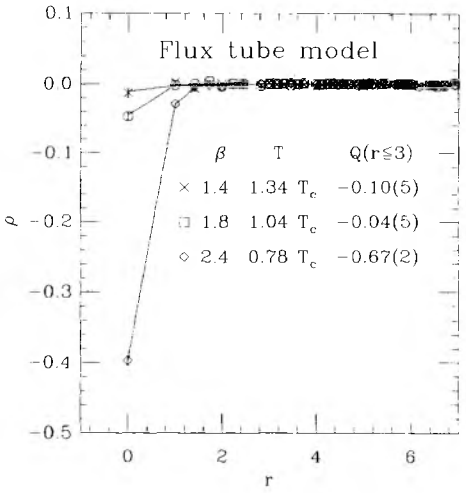

FIG. 11. Flux tube model with $m = 1.0$. Induced quark number density vs distance from the origin. The legend $Q(r \leq 3)$ gives the integral out to $r = 3$.

A companion simulation of the flux tube model has similar behavior and suggests an explanation. Heating past the crossover in this model results in an explosive growth of color singlet clusters. Thus at high temperature the addition of a single test quark has little effect on the ensemble, leading to an extremely weak correlation. We have an effective electrostatic deconfinement without a phase transition.

We also find that in the flux tube model baryonic clusters proliferate as the temperature rises through T_c, permitting more frequent baryonic screening of a test charge, suggesting an explanation for an apparent superabundance of baryons in full QCD at these temperatures. It is interesting to speculate that such a superabundance, particularly of antibaryons, should they survive final state interactions, provides an experimental signal for the crossover to the quark-plasma regime [13].

To be sure the flux tube model omits many features of QCD. It lacks dynamics, describing only electrostatics. It also ignores chiral symmetry. Completely omitted are the important magnetic interactions that give rise to confinement in spacelike propagation. It would be useful to find an elaboration of the model more closely relevant to QCD. Nonetheless, it is highly suggestive both for further exploration of QCD and for the phenomenology of the quark plasma.

ACKNOWLEDGMENTS

Code development and testing were carried out on the nCUBE and Intel iPSC/860 hypercubes at the San Diego Supercomputer Center. The QCD simulations were carried out on the Intel iPSC/860 at the NASA Ames Research Center and on the Thinking Machines Corporation CM5 at the National Center for Supercomputing Applications. The flux tube simulations were carried out on IBM RS6000/320 workstations in the Physics Department of the University of Utah. We wish to thank all of

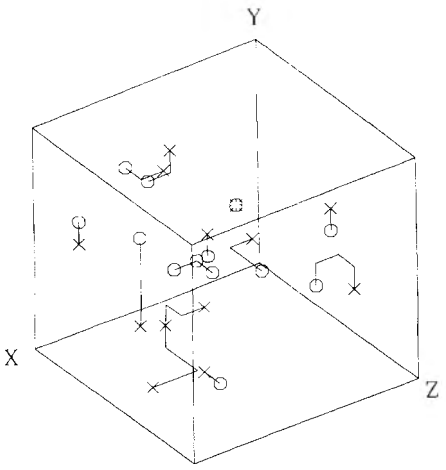

FIG. 10. Typical flux tube lattice at $T \approx 0.78\ T_c$. The origin, indicated by the burst, has been displaced for clarity.

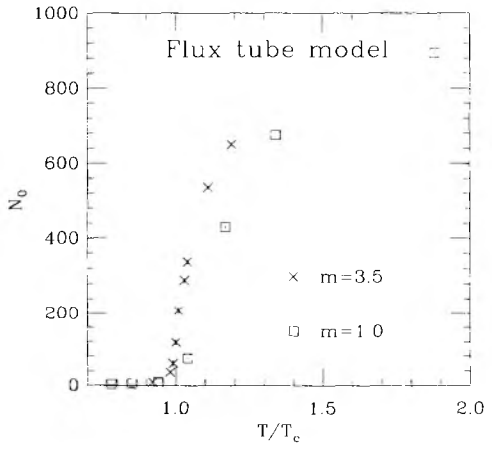

FIG. 12. Mean size of cluster connected to the origin vs inverse temperature for the flux tube model. The errors are smaller than the plot symbols.

these organizations for their support of our work. This research was supported in part by Department of Energy Grants Nos. DE-2FG02-91ER–40628, DE-AC02-84ER-40125, DE-AC02-86ER-40253, DE-FG02-85ER-40213, DE-FG03-90ER-40546, DE-FG02-91ER-40661, and National Science Foundation Grants Nos. NSF-PHY90-08482, NSF-PHY93-09458, NSF-PHY91-16964 and NSF-PHY91-01853.

[1] S. Gottlieb, W. Liu, R. Renken, R.L. Sugar, and D. Toussaint, Phys. Rev. D **35**, 3972 (1987); F. Karsch and H.W. Wyld, Phys. Lett. B **213**, 505 (1988); F. Karsch, in *Lattice '88*, Proceedings of the International Symposium, Batavia, Illinois, 1988, edited by A. S. Kronfeld and P. B. Mackenzie [Nucl. Phys. B (Proc. Suppl.) **9**, 357 (1989)].

[2] S. Gottlieb, W. Liu, R.L. Renken, R.L. Sugar, and D. Toussaint, Phys. Rev. Lett. **59**, 2247 (1987); Phys. Rev. D **38**, 2888 (1988).

[3] C. Bernard, T.A. DeGrand, C.E. DeTar, S. Gottlieb, A. Krasnitz, M.C. Ogilvie, R.L. Sugar, and D. Toussaint, Phys. Rev. Lett. **68**, 2125 (1992).

[4] C. Borgs, Nucl. Phys. **B261**, 455 (1981); E. Manousakis and J. Polonyi, Phys. Rev. Lett. **58**, 847 (1987); L. Kärkkäinen *et al.*, "Spacelike Wilson Loops at Finite Temperature," Bielefeld Report No. BI-TP-93-12 (unpublished); G.S. Bali, J. Fingberg, U.M. Heller, F. Karsch, and K. Schilling, Phys. Rev. Lett. **71**, 3059 (1993).

[5] M. Müller, M. Faber, W. Feilmair, and H. Markum, Nucl. Phys. **B335**, 502 (1990); W. Bürger, M. Faber, H. Markum, and M. Müller, Phys. Rev. D **47**, 3034 (1993).

[6] C. Bernard, T.A. DeGrand, C. DeTar, S. Gottlieb, A. Krasnitz, R.L. Sugar, and D. Toussaint, in *Lattice '92*, Proceedings of the International Symposium, Amsterdam, The Netherlands, 1992, edited by J. Smit and P. van Baal [Nucl. Phys. B (Proc. Suppl.) **30**, 319 (1993)].

[7] A. Patel, Nucl. Phys. **B243**, 411 (1984); Phys. Lett. **139B**, 394 (1984).

[8] J. Kogut, H. Matsuoka, M. Stone, H.W. Wyld, S. Shenker, J. Shigemitsu, and D.K. Sinclair, Nucl. Phys. **B225**, 93 (1983); P. Hasenfratz and F. Karsch, Phys. Lett. **125B**, 308 (1983); C. DeTar and T.A. DeGrand, Nucl. Phys. **B225**, 590 (1983).

[9] C. Bernard, T.A. DeGrand, C.E. DeTar, S. Gottlieb, A. Krasnitz, M.C. Ogilvie, R.L. Sugar, and D. Toussaint, Phys. Rev. D **45**, 3854 (1992).

[10] C. Bernard, T. Blum, T.A. DeGrand, C.E. DeTar, S. Gottlieb, A. Krasnitz, R.L. Sugar, and D. Toussaint, Phys. Rev. D **48**, 4419 (1993).

[11] C. DeTar and T. DeGrand, Nucl. Phys. **B225**, 590 (1983).

[12] L.G. Yaffe and B. Svetitsky, Phys. Rev. D **26**, 963 (1982); A.M. Polyakov, Phys. Lett. **72B**, 477 (1978); L. Susskind, Phys. Rev. D **20**, 2610 (1979).

[13] T. A. DeGrand, Phys. Rev. D **30**, 2001 (1984); J. Ellis and H. Kowalski, Phys. Lett. B **214**, 161 (1988); J. Ellis, U. Heinz, and H. Kowalski, *ibid.* **233**, 223 (1989); A.H. Mueller, in *Proceedings of the 7th International Conference on Ultrarelativistic Nucleus-Nucleus Collisions, Quark Matter, Lenox, 1988*, edited by G. Baym, P. Braun-Munzinger, and S. Nagamiya (North-Holland, Amsterdam, 1989); U. Heinz, P.R. Subramanian, W. Greiner, Z. Phys. A **318**, 247 (1984), J. Phys. G **12**, 1237 (1986); P. Koch, B. Müller, H. Stöcker, and W. Greiner, Mod. Phys. Lett. A **3**, 737 (1988).